

# Structural and electronic properties of $\text{Sr}_2\text{RuO}_4$ - $\text{Sr}_3\text{Ru}_2\text{O}_7$ heterostructure

Carmine Autieri

*SPIN-CNR, I-84084 Fisciano (Salerno), Italy*

*Dipartimento di Fisica "E. R. Caianiello", Università di Salerno, I-84084 Fisciano (Salerno), Italy and  
IAS, Forschungszentrum Jülich, 52425 Jülich, Germany*

Mario Cuoco and Canio Noce

*SPIN-CNR, I-84084 Fisciano (Salerno), Italy and*

*Dipartimento di Fisica "E. R. Caianiello", Università di Salerno, I-84084 Fisciano (Salerno), Italy*

By means of first-principles calculations we study the structural and electronic properties of a superlattice made of  $\text{Sr}_2\text{RuO}_4$  and  $\text{Sr}_3\text{Ru}_2\text{O}_7$  ruthenate oxides. Due to the symmetry mismatch of the two systems a significant structural rearrangement occurs within the superlattice. We find that at the interface the  $\text{RuO}_6$  octahedra get elongated for the  $\text{Sr}_2\text{RuO}_4$  while tend to be compressed for the  $\text{Sr}_3\text{Ru}_2\text{O}_7$  as compared to inner layers and the bulk phases. The positions of the Sr-atoms in the Sr-O layers at the interface are strongly modified and influence the alignment of the Ru atoms with respect to the planar oxygens as well as the Ru-O-Ru in-plane bond angles. Such structural rearrangement leads to a modification of the electronic structure close to the Fermi level. The main changes occurring at the interface and in the inner layers of the heterostructure are analyzed and compared with the bulk phases of the  $\text{Sr}_2\text{RuO}_4$  and  $\text{Sr}_3\text{Ru}_2\text{O}_7$  compounds. We show that the positions of the peaks in the density of states close to the Fermi levels get shifted and renormalized in the spectral weight. The balance between the renormalization of the bandwidth of the  $d_{xy}$  band and that of the crystal field splitting results into a minor change of the Van Hove singularities position within the superlattice. The effective tight-binding parameters for the  $4d$  Ru bands are determined by means of a maximally localized Wannier functions approach and used to discuss the modification of the electronic structure of the superlattice with respect to the bulk phases. Consequences on the modification of the superconducting and metamagnetic behaviour of the superlattice with respect to the bulk phases are discussed.

PACS numbers: 71.10.Fd 71.10.-w 75.10.Lp

## I. INTRODUCTION

There is a consolidated evidence that the interface between different electronic states and quantum orders is a source of novel physical phenomena<sup>1</sup>. The interest for this research area points both to the underlying fundamental physics as well as to the high impact in applications based on heterostructures with new emergent functionalities with respect to their constituents. Transition metal oxides (TMO) with perovskite structure are prototype systems to be exploited in this framework due to the large variety of correlated driven physical phenomena they exhibit, ranging from Mott insulator to unconventional superconductivity through all sorts of different spin-charge-orbital broken symmetry states<sup>2</sup>. Such aspect together with the recent achievements in the fabrication of atomically controlled TMO-based interfaces explain why they represent a unique laboratory to explore how spin, charge and orbital reconstruction at the interface may determine novel quantum states of matter<sup>3-9</sup>. On a general ground the reduced dimensionality at the interface is certainly a key driving force as it may enhance the electronic correlations against the kinetic energy. On the other hand, at a microscopic level it is the degree of matching of the TMO forming the heterostructure, the character of the transition elements and how they get into contact at the interface to be a complex source of a wide variety of physical properties.

In this context, the Ruddlesden-Popper (RP) family  $\text{Sr}_{n+1}\text{Ru}_n\text{O}_{3n+1}$  of Sr-based ruthenates, with  $n$  being the number of RuO layers in the unit cell, offers a distinct perspective for designing interfaces of TMOs made of homologue chemical elements but having a mismatch into the level of unit cell complexity and in the character of the broken symmetry states they exhibit as a function of  $n$ . The Sr-based RP family is made of itinerant correlated systems with tendency to superconducting or ferro- and meta-magnetic instabilities. The  $\text{Sr}_2\text{RuO}_4$   $n=1$  member is a spin-triplet superconductor with a topological non-trivial chiral pairing.<sup>10</sup> The  $n=2$  member,  $\text{Sr}_3\text{Ru}_2\text{O}_7$ , is an enhanced Pauli paramagnet<sup>11</sup> which at low-temperature exhibits an anisotropic metamagnetic (i.e. field-induced) transition, with possible emergent nematic states and unconventional quantum criticality.<sup>12,13</sup> Finally, the  $n=3$  member,  $\text{Sr}_4\text{Ru}_3\text{O}_{10}$ , shows ferro- or meta-magnetic behavior depending on the direction of the applied magnetic field,<sup>14-16</sup> and only  $\text{SrRuO}_3$  ( $n=\infty$ ) is an isotropic ferromagnetic metal with  $T_c \simeq 160$  K.<sup>17</sup>

There are two reasons that make quite unique the use of ruthenates RP-members in the interface design. First, the presence of an eutectic point in the chemical phase diagram of the SrRuO perovskites allows one to get natural interfaces in the form of single crystalline micrometric domains between adjacent members of the series, for instance  $\text{Sr}_2\text{RuO}_4$ - $\text{Sr}_3\text{Ru}_2\text{O}_7$  (i.e.  $n=1$  with  $n=2$ )<sup>18</sup>. Interestingly, for the eutectic systems interfaces between

the two RP members may also occur at the nanometer scale due to the intergrowth of the  $n=1$  phase in the form of stacking faults layers in the  $n=2$  domain and viceversa<sup>18,19</sup>. By means of the same growing technique, eutectic compounds of the type  $\text{Sr}_3\text{Ru}_2\text{O}_7\text{-Sr}_4\text{Ru}_3\text{O}_{10}$  (i.e.  $n=2$  with  $n=3$ ) have been also achieved<sup>20</sup> leading to interfaces between unit cells mad of RuO bilayers and trilayers. The investigation of the collective behavior of the eutectic phases indicates a relevant role of the interface physics as the superconducting<sup>21-23</sup> and the magnetic properties turn out to be quite different if compared to the homogeneous single crystalline ones. For instance, the  $\text{Sr}_2\text{RuO}_4\text{-Sr}_3\text{Ru}_2\text{O}_7$  eutectic shows an increase of the superconducting transition temperature  $T_c$ <sup>21</sup> while for the  $\text{Sr}_3\text{Ru}_2\text{O}_7\text{-Sr}_4\text{Ru}_3\text{O}_{10}$  there occurs a shift in the metamagnetic critical field. Such observations seem to point towards a significant electronic reconstruction at the interface between the different members of the RP-series which in turn results into a modification of the mechanisms responsible of the observed quantum phases.

Another aspect of the research interest for interfaces made of Sr-based ruthenates is that thin films of the series from  $n=1$  to  $n=5$ <sup>24,25</sup> have been successfully grown. Thus, the synthesis of superlattices based on different RP-members is an achievable task. In this framework, while the magnetic states are usually obtained in the Sr-RP members in the shape of thin films, it is quite remarkable to underline the recent preparation<sup>26</sup> of superconducting thin films of  $\text{Sr}_2\text{RuO}_4$  whose difficulty resides into the strong sensitivity of the spin-triplet pairing to disorder. This increases the research potential in designing superlattices or heterostructures by fully employing the different character of the broken symmetry states realized within the Sr-RP members as a function of  $n$ .

Taking into account the above mentioned motivations, the aim of the paper is to analyze the structural and electronic properties of  $\text{Sr}_2\text{RuO}_4\text{-Sr}_3\text{Ru}_2\text{O}_7$  superlattices. We use a first-principles density functional theory to determine the fully relaxed volume and the intra unit cell atomic positions as well as the electronic structure of heterostructure made with  $n=1$  and  $n=2$  unit cells. The Maximally Localized Wannier functions approach is then applied to extract the effective tight-binding parameters between the  $4d$  Ru orbitals in the superlattice at the interface and within the  $\text{Sr}_2\text{RuO}_4$  and  $\text{Sr}_3\text{Ru}_2\text{O}_7$  unit cells. The outcome is used to discuss the modification of the electronic structure of the superlattice, as well as its interrelation with the structural properties and the bulk phases. The focus is on two superlattice structures, as shown in Fig. 1(c)-(d), of the type  $(\text{Sr}_2\text{RuO}_4)_l\text{-(Sr}_3\text{Ru}_2\text{O}_7)_m$  with  $(l, m)=(3, 3)$  and  $(4, 2)$ ,  $l$  and  $m$  being the number of  $n=1$  and  $n=2$  unit cells in the heterostructure, respectively. Such configurations consist of at least an interface layers block that is inequivalent to the inner one within the  $n=1$  or the  $n=2$  side of the heterostructure. This allows one to extract the structural and the electronic features of the different Ru-O layers depend-

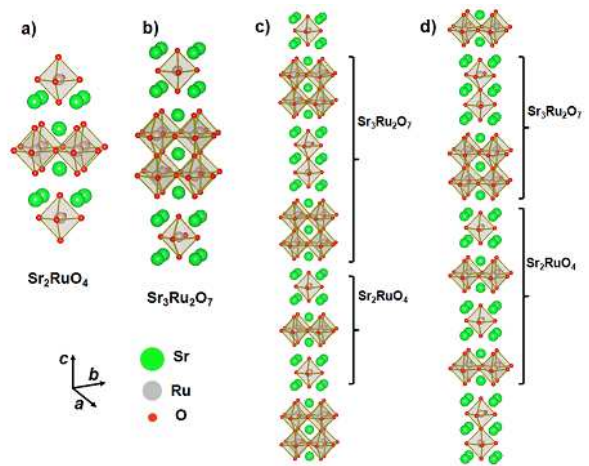


FIG. 1: Structure of the a)  $\text{Sr}_2\text{RuO}_4$ , b)  $\text{Sr}_3\text{Ru}_2\text{O}_7$  bulk phases as well as of the c)  $(\text{Sr}_2\text{RuO}_4)_3\text{-(Sr}_3\text{Ru}_2\text{O}_7)_3$  and d)  $(\text{Sr}_2\text{RuO}_4)_4\text{-(Sr}_3\text{Ru}_2\text{O}_7)_2$  superlattices.

ing on the character of the neighboring ones. Due to the different symmetry and size of the  $n=1$  and  $n=2$  unit cells a rearrangement of the atomic position takes place both within the Ru-O and Sr-O layers. We show that the  $\text{RuO}_6$  octahedra at the  $\text{Sr}_2\text{RuO}_4\text{-Sr}_3\text{Ru}_2\text{O}_7$  interface get elongated in the  $\text{Sr}_2\text{RuO}_4$  side and compressed in the  $\text{Sr}_3\text{Ru}_2\text{O}_7$  along the  $c$ -axis when compared to the inner layers block and to the bulk phases as well. The positions of the Sr atoms in the Sr-O layers get modified in a way to increase the Ru-O misalignment in the  $ab$  plane and result into an asymmetric planar bond length with respect to that with the apical oxygen. The interface layers undergo the major structural rearrangement which in turn influences the electronic structure close to the Fermi energy. Though the superlattice configuration would point to a greater change in the bands with  $d_{xz}$  and  $d_{yz}$  symmetry that mainly overlap along the  $c$ -axis, interesting variations are also observed for the  $d_{xy}$  band as due to the induced rotation of the  $\text{RuO}_6$  octahedra and the modification of the crystal field splitting. We show that the van Hove singularities of the  $\text{Sr}_2\text{RuO}_4$  and  $\text{Sr}_3\text{Ru}_2\text{O}_7$  bulk systems get shifted in energy in the superlattice and that such modification is more pronounced at the interface layers. As a signature of the hybridization between the  $n=1$  and  $n=2$  bands, there is a spectral weight enhancement for the  $d_{xy}$  band at energies which roughly correspond to those of the van Hove position in the  $\text{Sr}_3\text{Ru}_2\text{O}_7$ .

The paper is organized as follows. In the Sect. II we provide the general framework of the computational analysis. Sect. III is devoted to the presentation of the results concerning the structural and the electronic outcome for the  $\text{Sr}_2\text{RuO}_4$ ,  $\text{Sr}_3\text{Ru}_2\text{O}_7$  bulk phases as well as for the  $(\text{Sr}_2\text{RuO}_4)_l\text{-(Sr}_3\text{Ru}_2\text{O}_7)_m$  superlattices. In the Sect. IV we present the concluding remarks.

## II. COMPUTATIONAL FRAMEWORK

We perform unpolarized first-principles density functional calculations<sup>27</sup> by using the plane wave ABINIT package,<sup>28</sup> the Generalized Gradient Approximation (GGA) for the exchange-correlation functional,<sup>29</sup> and ultrasoft pseudopotentials.<sup>30</sup> We consider a plane-wave energy cut-off of 80 Ry and a cold smearing of 0.045 Ry. These values are common to all the presented calculations. The strategy we apply is to first perform the calculation of the relaxed crystal structure and of the energy spectra for the  $\text{Sr}_2\text{RuO}_4$  and  $\text{Sr}_3\text{Ru}_2\text{O}_7$  bulk phases and then to implement the same computational scheme for the superlattice. Since similar calculations have been already performed and a lot of data are available on the structural and electronic properties of the  $\text{Sr}_2\text{RuO}_4$  and  $\text{Sr}_3\text{Ru}_2\text{O}_7$  bulk phases, we have profited of such know-how to test the accuracy of the used approach. In this way, we feel confident to have a controlled scheme of analysis for the homogeneous and the superlattice structures. We would like to notice that standard functionals based on local density approximation may tend to overestimate the volume producing inaccurate ratio between the  $c$ - and  $a$ -axes.<sup>31</sup> This problem is encountered for the analyzed class of ruthenate oxides, especially for the  $\text{Sr}_3\text{Ru}_2\text{O}_7$  bulk phase. Thus, to get a more accurate determination of the volume and lattice constants in the study of the superlattice made of the first two RP members of the series, we employ the exchange-correlation of Wu and Cohen,<sup>29</sup> a variant of the generalized gradient approximation by Perdew *et al* (PBE)<sup>32</sup> method optimized for the relaxation of bulk systems. An  $8 \times 8 \times 8$  k-point grid is used for  $\text{Sr}_2\text{RuO}_4$ , while a  $8 \times 8 \times 2$  grid used for  $\text{Sr}_3\text{Ru}_2\text{O}_7$  for the full relaxation. Furthermore, the  $\text{Sr}_2\text{RuO}_4$ - $\text{Sr}_3\text{Ru}_2\text{O}_7$  hybrid structures are studied with a  $4 \times 4 \times 1$  k-point grid for the full relaxation and a  $8 \times 8 \times 1$  k-point grid for the determination of the density of states (DOS). We optimize the internal degrees of freedom by minimizing the total energy to be less than  $10^{-8}$  Hartree and the remaining forces to be less than  $10^{-4}$  Hartree/Bohr, and we require the external pressure to be less than 0.05 GPa to obtain the full relaxation of the system.

Let us consider some details about the determination of the effective tight-binding Hamiltonian in an atom-like Wannier basis for the  $\text{Sr}_2\text{RuO}_4$ ,  $\text{Sr}_3\text{Ru}_2\text{O}_7$  and the superlattice configurations. There are different ways to get the Wannier functions for the relevant electronic degrees of freedom including the orthogonalized projections of specific atomic orbitals on the Bloch wave-functions in a distinct energy window and downfolded muffin tin orbitals as well as maximally localized Wannier functions (MLFW). Hereafter, to extract the character of the electronic bands at the Fermi level, we use the Slater-Koster interpolation scheme based on the Maximally Localized Wannier Functions method (MLWF). Such approach is applied to the determination of the real-space Hamiltonian matrix elements in the MLWF basis for the bulk  $\text{Sr}_2\text{RuO}_4$  and  $\text{Sr}_3\text{Ru}_2\text{O}_7$  phases as well as for the

different superlattice configurations and to discuss the modification of the relevant parameters with respect to the structural changes. After obtaining the DFT Bloch bands within GGA, the MLWFs are constructed using the WANNIER90 code<sup>33</sup>. Starting from an initial projection of atomic  $d$  basis functions belonging to the  $t_{2g}$  sector and centered at the different Ru sites within the unit cell on the Bloch bands we get a set of three  $t_{2g}$ -like MLWF for each site within the different unit cells of the analyzed systems.

Then, we introduce the main concepts about the MLWFs procedure. We start by noticing that in general the Bloch waves can be expressed as a Bloch sum of atom-like basis functions or Wannier functions. Indeed, assuming to have a group of  $N$  Bloch states  $|\psi_{n\mathbf{k}}\rangle$  that is isolated in energy from the other bands in the Brillouin zone (BZ), one can construct a set of  $N$  localized Wannier functions  $|w_{n\mathbf{R}}\rangle$  associated with a lattice vector  $\mathbf{R}$  by means of the following transformation:

$$|w_{n\mathbf{R}}\rangle = \frac{V}{(2\pi)^3} \int_{BZ} \left( \sum_{m=1}^N U_{mn}^{(\mathbf{k})} |\psi_{m\mathbf{k}}\rangle \right) e^{-i\mathbf{k}\cdot\mathbf{R}} d\mathbf{k}$$

where,  $U^{(\mathbf{k})}$  is a unitary matrix that mixes the Bloch functions at a given  $\mathbf{k}$ -vector in the Brillouin zone. The choice of  $U^{(\mathbf{k})}$  determines the structure of the Wannier orbitals. In Ref.<sup>34</sup> the authors demonstrated that a unique set of Wannier functions can be obtained by minimizing the total quadratic spread of the Wannier orbitals expressed in terms of the position operator  $r$  through the following relation  $\Omega = \sum_{n=1}^N [\langle r^2 \rangle_n - \langle r \rangle_n^2]$  with  $\langle O \rangle_n = \langle w_{n0} | O | w_{n0} \rangle$ . For the case of entangled bands, one has to introduce another unitary matrix that takes into account the extra Bloch bands in the energy window upon examination. Such matrix is also obtained by minimizing the functional  $\Omega$ .<sup>35</sup> Once a set of MLWFs is determined the corresponding matrix Hamiltonian is given by a unitary transformation from the diagonal one in the Bloch basis. The resulting real space representation of the Hamiltonian in the MLWF basis can be expressed as

$$\tilde{H} = \sum_{\mathbf{R}, \mathbf{d}} t_{nm}^{\mathbf{d}} \left( \tilde{c}_{n, \mathbf{R}+\mathbf{d}}^\dagger \tilde{c}_{m, \mathbf{R}} + h.c. \right)$$

here  $\tilde{c}_{m, \mathbf{R}}$  destroy an electron in the  $n$  orbital Wannier state  $|w_{n\mathbf{R}}\rangle$ . Then, the real space elements  $t_{nm}^{\mathbf{d}}$  can be considered effective hopping amplitudes as in a tight-binding approach between MLWF separated by a distance  $\mathbf{d}$  associated with the lattice vectors. The index  $n$  refers to site and orbitals in the case of a unit cell that contains more than one site.

## III. RESULTS

In this section we present the structural and electronic properties of the  $\text{Sr}_2\text{RuO}_4$ - $\text{Sr}_3\text{Ru}_2\text{O}_7$  superlattice. Before considering the hybrid structure, we analyze the

electronic structure of the bulk  $\text{Sr}_2\text{RuO}_4$  and  $\text{Sr}_3\text{Ru}_2\text{O}_7$  phases within the computation scheme above mentioned. We remind that  $\text{Sr}_2\text{RuO}_4$  has a space group  $I4/mmm$ , whereas, due the rotations of the octahedra,  $\text{Sr}_3\text{Ru}_2\text{O}_7$  presents an orthorhombic symmetry with  $Pbn$  space group.

### 1. Bulk $\text{Sr}_2\text{RuO}_4$ phase

The electronic structure of  $\text{Sr}_2\text{RuO}_4$  has been already studied by several authors by means of density functional theory with Local Density Approximation (LDA) or GGA.<sup>36–40</sup> The tetravalent Ru atom has four electrons left in the  $4d$  shell; the quasi-cubic crystal field splits the  $d$  levels into three-fold degenerate  $t_{2g}$  and two-fold degenerate  $e_g$  states. At the Fermi level, four electrons fill the  $t_{2g}$  bands, while the  $e_g$  bands are empty, being higher in energy. DFT calculations show that the three  $t_{2g}$  bands can be divided into a wider quasi-two-dimensional  $xy$ , and two quasi-one-dimensional bands of  $\gamma z$  character. While the first band does not hybridize with the others, the  $xz$  and  $yz$  mix each other by forming an electron and hole-like Fermi sheets.

The electronic structure and the dispersion calculated from the  $t_{2g}$ -like MLWFs are shown in Fig. 2. The spectra and the derived Fermi surface is in agreement with those of the previous studies. As a distinct feature that will be also analyzed later on for the superlattice we notice that the energy spectrum exhibits a flatness at the  $M = (0, \pi)$  and  $(\pi, 0)$  points of the Brillouin zone leading to a van Hove singularity in the density of states above the Fermi level. The MLWFs approach provides the effective electronic parameters for the  $t_{2g}$ -atomiclike obtained Wannier functions. The resulting amplitudes are reported in the Table I along specific connecting vectors in the  $ab$  plane and along the  $c$ -axis. The amplitude of the effective electronic parameters is in agreement with those deduced by means of different first principles methods.<sup>40</sup>

We point out that DFT calculations based on LDA<sup>36–38</sup> place the  $(\pi, 0)$ ,  $(0, \pi)$  saddle point of the  $xy$  band about 60 meV above the Fermi energy. By taking into account the gradient corrections this singularity is lowered in energy to about 50 meV above the Fermi level,<sup>38</sup> while local Coulomb correlations push the  $xy$  VHS approximately to within 10 meV, near the Fermi energy.<sup>39,40</sup>

Concerning the structural properties, the relaxed in-plane (out-of-plane) lattice constant  $a$  ( $c$ ) turns out to be slightly larger (smaller) than the available experimental value with a resulting computed volume which is only  $\sim 0.7\%$  larger than the experimental one. For completeness, it is worth pointing out that the volume obtained using PBE is  $\sim 1\%$  larger than experimental value.<sup>41</sup>

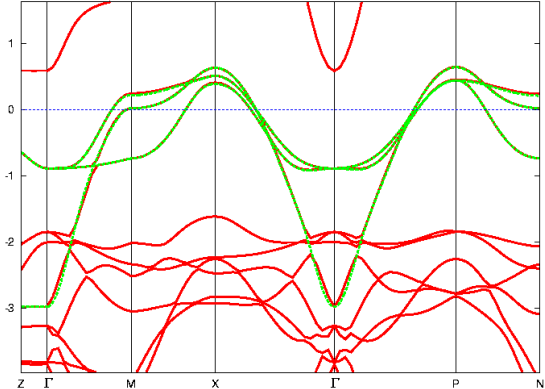


FIG. 2: Electronic structure of  $\text{Sr}_2\text{RuO}_4$  obtained within the density functional analysis by means of GGA (red full line) and the dispersion obtained from the  $t_{2g}$ -like MLWFs (green dotted line). The  $e_g$  levels are about 0.5 eV above the Fermi level. The Fermi level is set to zero and the energies are reported in eV.

### 2. Bulk $\text{Sr}_3\text{Ru}_2\text{O}_7$ phase

The electronic structure of  $\text{Sr}_3\text{Ru}_2\text{O}_7$  has been analyzed using ARPES<sup>42,43</sup> and density functional calculations<sup>44</sup> with a reasonable agreement between theory and experiments. Due to the presence of two RuO layers in the unit cell, as compared with the  $\text{Sr}_2\text{RuO}_4$  case, there are replica of the  $t_{2g}$  bands which are then split by the bilayer coupling and the orthorhombic distortions. To a first approximation the Fermi surface of the  $\text{Sr}_3\text{Ru}_2\text{O}_7$  can be derived from the six  $t_{2g}$  bands (three from each RuO layer) with bonding-antibonding (odd-even) splitting due to the bilayer coupling. Nevertheless the topology of the Fermi surface is deeply modified with respect to a simple doubling of the Fermi sheets due to various factors. The bilayer splitting, the extra  $k_z$  dispersions, and the avoiding crossing between the  $d_{xy}$  and the  $d_{\gamma z}$  bands tend to reduce the bands nesting. Furthermore, due to the orthorhombic distortions, small cylindrical lens shaped Fermi sheets form around the M point (i.e. the midpoint of the original  $\Gamma$  to X direction in the tetragonal Brillouin zone) and two small cylindrical sheets with almost no  $k_z$  dispersion around the  $\Gamma$  point.

We have performed a detailed analysis of the electronic structure of the bilayer  $\text{Sr}_3\text{Ru}_2\text{O}_7$  within the GGA scheme described in the Sect. II by focusing on the case of the fully distorted orthorhombic configuration.<sup>45</sup> The obtained band structure reported in Fig. 3 as well as the derived Fermi surface fairly agree with the ARPES and the previous density functional results above mentioned. Due to the various physical factors that enter into the electronic structure and the difficulty to trace and correlate them when a superlattice configurations is considered, we have determined the effective tight-binding



TABLE I: Hopping integrals along the direction  $[lmn]$  and on-site energy in eV associated to the three orbitals of the  $t_{2g}$  sector of the bulk  $\text{Sr}_2\text{RuO}_4$  at experimental atomic positions<sup>48</sup>. The connecting vector is expressed in terms of the integer set  $[lmn]$  and the lattice constants  $a$  and  $c$  as  $\mathbf{d} = l\mathbf{a}\mathbf{x} + m\mathbf{a}\mathbf{y} + n\mathbf{c}\mathbf{z}$ .<sup>28,33,49</sup>

orbital index	amplitude							
	$[000]$	$[100]$	$[010]$	$[110]$	$[200]$	$[020]$	$[\frac{1}{2}\frac{1}{2}\frac{1}{2}]$	$[001]$
xy-xy	-0.4750	-0.3867	-0.3867	-0.1384	0.0094	0.0094	0.0017	-0.0013
yz-xy	0	0	0	0	0	0	0.0057	0
xz-xy	0	0	0	0	0	0	0.0057	0
yz-yz	-0.3224	-0.0389	-0.2914	0.0165	0.0010	0.0612	-0.0188	0.0006
yz-xz	0	0	0	-0.0121	0	0	-0.0136	0
xz-xz	-0.3224	-0.2914	-0.0389	0.0165	0.0612	0.0010	-0.0188	0.0006

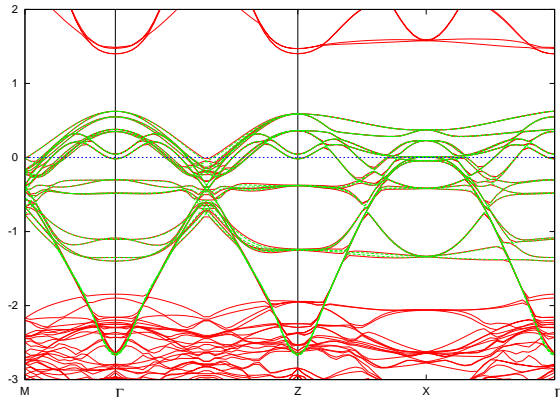


FIG. 3: Electronic structure of  $\text{Sr}_3\text{Ru}_2\text{O}_7$  obtained within the density functional analysis by means of GGA (red full line) and the dispersion obtained from the  $t_{2g}$ -like MLWFs (green dotted line). The position of the Van Hove like singularity is located in the middle of the long direction Z- $\Gamma$  (X point). The position of the VHS is the same of  $\text{Sr}_2\text{RuO}_4$ , but, the crystal symmetry is different. The Fermi level is set to zero and the unit scale of the energies is eV.

parameters in the MLWFs basis.

In a tetragonal environment the MLWFs mainly correspond with the  $t_{2g}$ -atomiclike states, and this is the case for the  $\text{Sr}_2\text{RuO}_4$ . However, the MLWFs for the  $\text{Sr}_3\text{Ru}_2\text{O}_7$  are different because the rotation of the octahedra slightly modifies their character by leading to a small charge redistribution following the distortion of the orthorhombic structure. In particular, this misalignment turns out to be more pronounced for the MLWFs which has an orbital distribution with  $d_{xy}$  symmetry. Similar conclusions have been also reported in Ref. 47. The effective electronic parameters for the  $\text{Sr}_3\text{Ru}_2\text{O}_7$  based on the  $t_{2g}$ -like MLWFs are reported in Table II. There are different aspects that can be noticed when comparing the effective hopping of the  $\text{Sr}_2\text{RuO}_4$  with those of the  $\text{Sr}_3\text{Ru}_2\text{O}_7$ . The first observation is that the nearest-neighbor hopping for the  $d_{xy}$  orbital in the distorted structural configuration is reduced with respect to the ideal tetragonal case and matches with that one for the

$d_{xz}$  and  $d_{yz}$  states. The reduction for the  $d_{xy}$  orbital can be also phrased in a Slater and Koster scheme<sup>46</sup>. Indeed, the integral overlap  $E_{d_{xy},p_x}$  between the  $d_{xy}$  orbital on Ru and the 2p orbital on O reduces when there is a modification of the angle between the Ru and O atoms. Since the effective Ru-Ru hopping between the  $d_{xy}$  orbitals  $t_{xy,xy}^{100}$  depends on the amplitude  $E_{d_{xy},p_x}$  the reduction expected from the Slater and Koster approach is consistent with the result obtained within the MLWFs approach. As an indirect consequence of the change of the  $xy$  nearest neighbor hopping, the VHS moves below the Fermi level as shown in Fig. 3.

Then, one can notice that the Ru-Ru hybridization via the  $d_{xy}$  orbital occur both within the bilayer and also for the second-nearest neighbor in the RuO layers. The  $d_{xy}$  orbital exhibits also non negligible overlap with the  $d_{xz}$  and  $d_{yz}$  within the RuO layers. Such hybridization processes are identically zero by symmetry in the  $\text{Sr}_2\text{RuO}_4$  system and thus represents a relevant contribution in the determination of the electronic structure and consequently the Fermi surface topology for the  $\text{Sr}_3\text{Ru}_2\text{O}_7$ . Concerning the  $c$ -axis dispersion, the  $\gamma z$  orbitals have a larger overlap across the bilayers if compared to the  $\text{Sr}_2\text{RuO}_4$  system.

Finally, concerning the structural analysis, looking at Table III we find out that the  $a$  lattice constant almost coincides with the experimental value, while the experimental  $c$  lattice constant is slightly lower than the numerical value. Also in this case, the theoretical volume is  $\sim 0.7\%$  larger than the experimental one.

### 3. $\text{Sr}_2\text{RuO}_4$ - $\text{Sr}_3\text{Ru}_2\text{O}_7$ superlattice: structural properties

In this subsection we consider the structural properties of the  $\text{Sr}_2\text{RuO}_4$ - $\text{Sr}_3\text{Ru}_2\text{O}_7$  superlattices. The fully relaxed volume and the intra unit cell atomic positions have been determined for the two superlattices, shown in Fig. 1(c)-(d), of the type  $(\text{Sr}_2\text{RuO}_4)_l$ - $(\text{Sr}_3\text{Ru}_2\text{O}_7)_m$  with  $(l, m) = (3, 3)$  and  $(4, 2)$ , where  $l$  and  $m$  are the number of  $n=1$  and  $n=2$  unit cells in the heterostructure. Hereafter we denote as HET42 and HET33 the two superlattice

TABLE II: Effective hopping parameters along the direction  $[lmn]$  and on-site energy in eV associated to the  $t_{2g}$ -like Wannier functions for the  $\text{Sr}_3\text{Ru}_2\text{O}_7$ . The connecting vector is expressed in terms of the integer set  $[lmn]$  and the lattice constants  $a$  and  $c$  as  $\mathbf{d} = la\mathbf{x} + ma\mathbf{y} + nc\mathbf{z}$  <sup>28,33,49</sup>. The direction  $00p$  connect the two ruthenium atoms in the bilayer. The hopping parameters that are zero in the tetragonal phase have sign dependent from the tilting (clockwise or anticlockwise). The hopping parameters  $t^{\frac{1}{2}\frac{1}{2}\frac{1}{2}}$  can have different connections: depending on the character of the rotation of the two octahedra the hopping parameter can increase, decrease or be similar in amplitude to those obtained for the  $\text{Sr}_2\text{RuO}_4$  compound.

orbital index	amplitude							
	[000]	[100]	[010]	[110]	[200]	[020]	$[\frac{1}{2}\frac{1}{2}\frac{1}{2}]$	[00p]
xy-xy	-0.482	-0.292	-0.292	-0.134	-0.021	-0.021	0.002/0.001	-0.018
yz-xy	0	$\pm 0.001$	$\pm 0.010$	$\pm 0.001$	$\pm 0.002$	$\pm 0.006$	0.006/0.005/0.004	0
xz-xy	0	$\pm 0.010$	$\pm 0.001$	$\pm 0.001$	$\pm 0.006$	$\pm 0.002$	0.006/0.005/0.004	0
yz-yz	-0.386	-0.020	-0.301	0.014	0.002	0.041	-0.023/-0.018/-0.014	-0.264
yz-xz	0	$\pm 0.061$	$\pm 0.061$	-0.013	$\pm 0.007$	$\pm 0.007$	-0.024/-0.015/-0.006	0
xz-xz	-0.386	-0.301	-0.020	0.014	0.041	0.002	-0.023/-0.018/-0.014	-0.264

TABLE III: Comparison between the experimental and theoretical estimation of the lattice constants for the  $\text{Sr}_2\text{RuO}_4$  and the  $\text{Sr}_3\text{Ru}_2\text{O}_7$ . The length unit is in angstrom.

	Exp. $\text{Sr}_2\text{RuO}_4$ <sup>48</sup>	Th. $\text{Sr}_2\text{RuO}_4$	Exp. $\text{Sr}_3\text{Ru}_2\text{O}_7$ <sup>45</sup>	Th. $\text{Sr}_3\text{Ru}_2\text{O}_7$	$(\text{Sr}_2\text{RuO}_4)_4$ - $(\text{Sr}_3\text{Ru}_2\text{O}_7)_2$	$(\text{Sr}_2\text{RuO}_4)_3$ - $(\text{Sr}_3\text{Ru}_2\text{O}_7)_3$
$a$	3.862	3.887	3.873	3.872	3.881	3.869
$c$	12.723	12.650	20.796	20.968	46.234	50.554

structures with  $(l, m)=(4, 2)$  and  $(3, 3)$ , respectively.

As a first outcome of the structural analysis, we have compared the lattice constants of the  $n=1$  and  $n=2$  bulk phases with the ones obtained by the full relaxation of the HET42 and HET33. The results are reported in Table III and include also the comparison with the experimental data for the available compounds. When the HET42 and HET33 configurations are considered, we find that the HET42  $a$  lattice constant has an intermediate value between the amplitude of the  $\text{Sr}_2\text{RuO}_4$  and  $\text{Sr}_3\text{Ru}_2\text{O}_7$  bulk phases. Otherwise, for the case of the HET33 superlattice, where the number of  $\text{Sr}_3\text{Ru}_2\text{O}_7$  cells is increased,  $a$  gets further reduced if compared to the theoretical values obtained for the pure  $\text{Sr}_2\text{RuO}_4$  and  $\text{Sr}_3\text{Ru}_2\text{O}_7$ . Such modification of the in-plane lattice constants influences the dimension of the unit cell along the  $c$ -axis by leading to an overall elongation.

The analysis of the atomic positions provides indications of the rearrangement of the atoms within the  $\text{Sr}_2\text{RuO}_4$  and  $\text{Sr}_3\text{Ru}_2\text{O}_7$  sides of the superlattice. From the inspection of the Tables IV and V we are able to extract all the relevant information concerning the distortions and rotations of the  $\text{RuO}_6$  octahedra in the superlattice. In particular, due to the  $c$ -axis mismatch between the  $n=1$  and  $n=2$  systems the shorter (longer) unit cell gets elongated (flattened) to optimally adapt within the heterostructure. Consequently the Ru-O distances are modified in such a way that the octahedra are elongated in the  $\text{Sr}_2\text{RuO}_4$  and flattened in the  $\text{Sr}_3\text{Ru}_2\text{O}_7$  side of the superlattice if compared to the corresponding bulk

phases. Such distortions are not uniform because the main changes occur at the  $\text{Sr}_2\text{RuO}_4$ - $\text{Sr}_3\text{Ru}_2\text{O}_7$  interface while in the inner layers the octahedra relax at bond lengths which match those of the bulk systems. Assuming the notation in Fig. 4a, the Ru- $O_{in}$  distance in the  $\text{Sr}_3\text{Ru}_2\text{O}_7$  does not change for the superlattice HET42 but it grows for the HET33 structure. The growth occurs both in the inner side and at the interface of the superlattice. However, at the interface the distance Ru- $O_{in}$  increases respect to the inner layers in both cases. The bond lengths involving the Sr-atoms and the surrounding oxygens are also modified in the superlattice if compared to the bulk phases. The major changes are observed in the  $\text{Sr}_3\text{Ru}_2\text{O}_7$  side of the superlattice where the Sr-O bonds have the tendency to increase with respect to the bulk values.

To complete the structural analysis, we have considered the  $\Delta z$  displacement along the  $c$ -axis of the Ru atoms with respect to the planar oxygens, and the variation of the Ru-O-Ru bond angles. The results are summarized in Table V from which we can infer two different trends for  $\Delta z$  in  $\text{Sr}_2\text{RuO}_4$  and  $\text{Sr}_3\text{Ru}_2\text{O}_7$ . Indeed, as far as  $\Delta z$  for  $\text{Sr}_2\text{RuO}_4$  is considered, we see that in the inner unit cells of both the HET42 and HET33 structures this quantity is zero, i. e. there is no variation of the displacement along the  $c$ -axis of Ru ions compared to the pure phase. On the other hand, at the interface a small  $\Delta z$  is produced and the Ru atom goes far from the interface as shown in Fig. 5. Concerning the  $\text{Sr}_3\text{Ru}_2\text{O}_7$ , a  $\Delta z$  is already present in the case of the bulk phase, but an

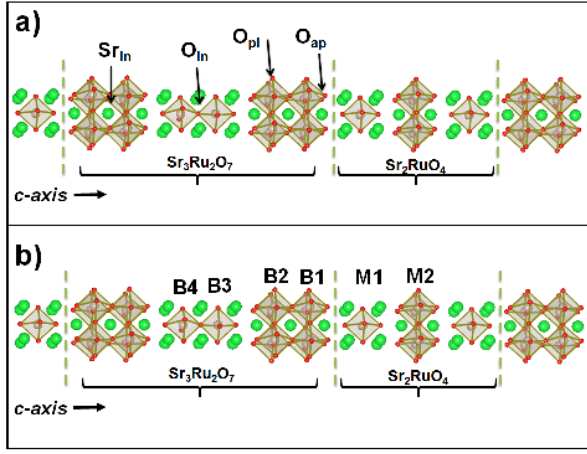


FIG. 4: Notation about the labelling of the atoms within the superlattice.  $O_{pl}$  is the planar oxygen,  $O_{ap}$  is the apical oxygen,  $O_{in}$  denotes the intra-bilayer oxygen, and  $Sr_{in}$  the intra-bilayer strontium.  $Sr_{in}$  and  $O_{in}$  are present only in the  $Sr_3Ru_2O_7$  side of the heterostructure. The remaining strontium atoms are labelled Sr.

enhancement of the amplitude of  $\Delta z$  is deduced at the interface.

Concerning the Ru-O-Ru bond angles there is no significant variation in the inner layers of the  $Sr_2RuO_4$  side of the superlattice for both the HET42 and HET33 configurations, while at the interface the displacement along the  $c$ -axis of the Ru atoms produces a reduction of the Ru-O-Ru angle. The situation is completely different for the  $Sr_3Ru_2O_7$  side of the hybrid structure. Indeed, a deviation from the pure phase angle is found, as well as in the inner region, exhibits a dependence whose amplitude is related to the size of considered superlattice. However, the bond angle increases respect to the inner region in both cases. The rotation angle of the octahedra, that is half of the Ru-O-Ru supplementary angle, decreases at the interface in the  $Sr_3Ru_2O_7$  phase.

On the basis of the results above discussed, we show how the atoms of  $Sr_2RuO_4$  and  $Sr_3Ru_2O_7$  rearrange at the interface, along the  $c$ -axis. The picture that emerges is shown in Fig. 5. The change of the atomic positions reveals a tendency of the ions positively charged in the ionic picture to move in the direction of the  $Sr_2RuO_4$  side, while the negative ones go in the opposite direction towards the  $Sr_3Ru_2O_7$  side. We notice that two bonds are strongly modified at the interface: the distance between the ruthenium and the apical oxygen, and the distance between the Sr ion and the apical oxygen along the  $c$ -axis, the other in-plane modifications being smaller.

#### 4. $Sr_2RuO_4$ - $Sr_3Ru_2O_7$ superlattice: electronic properties

We have determined the electronic properties of the  $(Sr_2RuO_4)_4$ - $(Sr_3Ru_2O_7)_2$  and  $(Sr_2RuO_4)_3$ - $(Sr_3Ru_2O_7)_3$

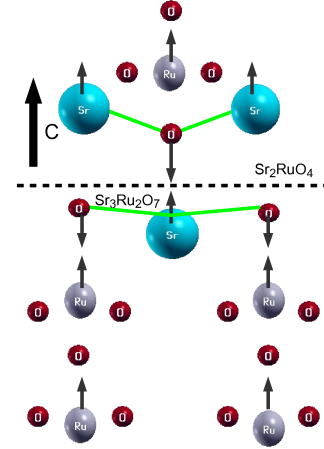


FIG. 5: Schematic view of the atomic rearrangement at the interface of the  $Sr_2RuO_4$ - $Sr_3Ru_2O_7$  heterostructure. The arrows indicate the most relevant displacements at the interface as compared to the inner layers. The different geometrical configuration of the Sr-O plane is shown (green line). It is more flat for  $Sr_3Ru_2O_7$ , while there is a greater difference between the Sr and the O atom along the  $c$ -axis in  $Sr_2RuO_4$ .

heterostructures with the aim to analyze the modifications of the spectra within the superlattice and in comparison with the bulk phases as well as to extract the interrelation between the structural changes and the electronic dispersions. Based on the detailed analysis of the structural properties we expect that the effective hopping and the hybridization parameters for the energy bands at the Fermi level are influenced both in the amplitude and in the character. Also a rearrangement of the on-site Ru  $4d$  energies is expected to influence the  $4d$  energy splitting due to the flattening and elongation of the  $RuO_6$  octahedra within the superlattice.

Since the unit cell is quite complex and contains many bands close to the Fermi level we have analyzed the projected density of states for the Ru  $t_{2g}$ -like orbitals as well as for the oxygen and Sr bands at the inner and the interface layers of the  $Sr_2RuO_4$  and  $Sr_3Ru_2O_7$  sides within the superlattice. Furthermore, in order to extract the relevant changes induced by the interface reconstruction and the structural distortions we have determined the effective tight-binding Hamiltonian in the MLWFs basis for the bands close to the Fermi level.

Let us consider the DOS for the Ru  $t_{2g}$ -like bands. The results are presented for the HET42 configuration. We have checked that the HET33 structure does not exhibit substantial qualitative differences. In Fig. 6 it is reported the DOS for the projected  $t_{2g}$ -like bands of Ru atoms placed at the interface and inner layers for the  $Sr_2RuO_4$  and  $Sr_3Ru_2O_7$  side of the superlattice for an energy window close to the Fermi level where the major changes occur. From a general view the DOS shows the features of the bulk  $Sr_2RuO_4$  and  $Sr_3Ru_2O_7$  for instance as far as it concerns the Van Hove like peaks below and

TABLE IV: Inequivalent atomic bonds length in bulk ruthenates and for the  $(\text{Sr}_2\text{RuO}_4)_4$ - $(\text{Sr}_3\text{Ru}_2\text{O}_7)_2$  and  $(\text{Sr}_2\text{RuO}_4)_3$ - $(\text{Sr}_3\text{Ru}_2\text{O}_7)_3$  superlattices. The inner layers are the RuO planes which have neighbors along the  $c$ -axis having the same unit cell. For instance, in Fig. 4b they are labelled as B3 and B4 for the  $\text{Sr}_3\text{Ru}_2\text{O}_7$  region, and M2 for the  $\text{Sr}_2\text{RuO}_4$  one. The interface layers are those at the boundary between the  $\text{Sr}_2\text{RuO}_4$  and  $\text{Sr}_3\text{Ru}_2\text{O}_7$  regions of the superlattice. In Fig. 4b they are denoted as B1 and B2 for the  $\text{Sr}_3\text{Ru}_2\text{O}_7$  region, and M1 for the  $\text{Sr}_2\text{RuO}_4$  one. There are empty spaces in the table because the corresponding values are not allowed for the given crystal structure.

	Exp. <sup>45,48</sup>	Th. Bulk	Inner layers HET42	Interface layers HET42	Inner layers HET33	Interface layers HET33
Ru- $O_{ap}$ in $\text{Sr}_2\text{RuO}_4$	2.062	2.059	2.059	2.069	2.068	2.076
Ru- $O_{ap}$ in $\text{Sr}_3\text{Ru}_2\text{O}_7$	2.038	2.059	2.058	2.050	2.063	2.056
Ru- $O_{pl}$ in $\text{Sr}_2\text{RuO}_4$	1.931	1.943	1.943	1.943	1.934	1.934
Ru- $O_{pl}$ in $\text{Sr}_3\text{Ru}_2\text{O}_7$	1.956	1.972	1.977	1.977	1.973	1.972
Ru- $O_{in}$ in $\text{Sr}_3\text{Ru}_2\text{O}_7$	2.026	2.045	2.043	2.045	2.049	2.052
Sr- $O_{ap}$ in $\text{Sr}_2\text{RuO}_4$ along $c$	2.429	2.433	2.433		2.431	
Sr- $O_{ap}$ in $\text{Sr}_3\text{Ru}_2\text{O}_7$ along $c$	2.452	2.449	2.455		2.447	
$\text{Sr}^{(n=2)}\text{-O}_{ap}^{(n=1)}$ along $c$				2.423		2.416
$\text{Sr}^{(n=1)}\text{-O}_{ap}^{(n=2)}$ along $c$				2.472		2.469
Sr- $O_{ap}$ in $\text{Sr}_2\text{RuO}_4$ in $ab$	2.738	2.757	2.757	2.758	2.745	2.747
Sr- $O_{ap}$ in $\text{Sr}_3\text{Ru}_2\text{O}_7$ in $ab$	2.744	2.743	2.755	2.755	2.739	2.740
Sr- $O_{pl}$ in $\text{Sr}_2\text{RuO}_4$	2.688	2.670	2.671	2.673	2.676	2.675
Sr- $O_{pl}$ in $\text{Sr}_3\text{Ru}_2\text{O}_7$	2.506/2.896	2.473/3.002	2.478/2.997	2.480/2.997	2.470/3.015	2.473/3.017
$\text{Sr}_{in}\text{-O}_{in}$	2.738	2.738	2.747	2.747	2.737	2.736
$\text{Sr}_{in}\text{-O}_{pl}$	2.607/2.986	2.548/3.064	2.556/3.062	2.553/3.055	2.545/3.074	2.543/3.068

TABLE V: Ru-O-Ru bond angles and displacement of Ru in the several case studied. At the interface, the modification of the Ru-O-Ru bond angle in  $\text{Sr}_2\text{RuO}_4$  it is due to the Ru displacement along the  $c$ -axis, no rotations are found.

	Exp. <sup>45,48</sup>	Th. Bulk	Inner RuO layers HET42	Interface HET42	Inner RuO layers HET33	Interface HET33
$\Delta z$ in $\text{Sr}_2\text{RuO}_4$	0	0	0	0.008	0	0.007
$\Delta z$ in $\text{Sr}_3\text{Ru}_2\text{O}_7$	0.017	0.033	0.032	0.039	0.030	0.037
Ru-O-Ru bond angle in $\text{Sr}_2\text{RuO}_4$	180.0°	180.0°	180.0°	179.5°	180.0°	179.6°
Ru-O-Ru bond angle in $\text{Sr}_3\text{Ru}_2\text{O}_7$	163.9°	158.1°	158.6°	158.8°	157.4°	157.5°

above the Fermi level for the  $d_{xy}$  bands and the one dimensional distribution of spectral weight for the  $\gamma z$  ones. One important aspect we notice is that, though the octahedra deformation is not uniform within the superlattice, the DOS does not exhibit significant shifts in energy when comparing the interface with the inner layers. This can be addressed by considering that the change in the crystal field and the modification of the effective bandwidth can balance and reduce the energy shifts within the superlattice. The analysis of the effective tight-binding parameters within the MLWFs reveal that indeed this is the case for the  $\text{Sr}_2\text{RuO}_4$ - $\text{Sr}_3\text{Ru}_2\text{O}_7$  heterostructure. Slight changes are visible only for the  $d_{xy}$  bands whereas in the  $\text{Sr}_3\text{Ru}_2\text{O}_7$  there is a small suppression of spectral weight below the Fermi level at the interface compared to the inner layers, the opposite occurs above the Fermi energy. The Ru  $d_{xy}$  DOS in the  $\text{Sr}_2\text{RuO}_4$  side of the superlattice exhibits a slight increase of the spectral weight at energies where a redistribution and an overlap of the

$d_{\gamma z}$  bands with the  $d_{xy}$  one occur in the  $\text{Sr}_3\text{Ru}_2\text{O}_7$  region. No significant variations can be noticed for the  $\gamma z$  bands across the superlattice.

More interesting is the comparison between the DOS of the superlattice and that one of the bulk  $\text{Sr}_2\text{RuO}_4$  and  $\text{Sr}_3\text{Ru}_2\text{O}_7$  systems. We focus on the variation of the VHS positions close to the Fermi level for the  $xy$  band. In Fig. 7 we present the  $d_{xy}$  DOS for the interface and inner layers of the HET42 superlattice for the  $\text{Sr}_2\text{RuO}_4$  and  $\text{Sr}_3\text{Ru}_2\text{O}_7$  sides in comparison with the corresponding bulk DOS. We notice that the peak associated with the VHS in the bulk  $\text{Sr}_3\text{Ru}_2\text{O}_7$  gets reduced and shifted towards the Fermi level in the  $\text{Sr}_3\text{Ru}_2\text{O}_7$ . This is mainly due to the change of the  $d_{xy}$  bandwidth and of the crystal field splitting driven by the rotation and flattening or elongation of the octahedra. On the other hand the VHS placed above the Fermi level in the  $\text{Sr}_2\text{RuO}_4$  is moved away from the Fermi level.

To understand more deeply the differences in the elec-



TABLE VI: Effective hopping parameters along the direction  $[lmn]$  and on-site energy in eV associated to the  $t_{2g}$ -like Wannier functions for the  $(\text{Sr}_2\text{RuO}_4)_3$ - $(\text{Sr}_3\text{Ru}_2\text{O}_7)_3$  superlattice. The connecting vector is expressed in terms of the integer set  $[lmn]$  and the lattice constants  $a$  and  $c$  as  $\mathbf{d} = la\mathbf{x} + ma\mathbf{y} + nc\mathbf{z}$  for the related subsystems. The direction  $00p$  connect the two ruthenium atoms within the bilayer of the  $\text{Sr}_3\text{Ru}_2\text{O}_7$  side of the superlattice. B1 and B2 indicate the RuO layers within the bilayer placed at the interface with the  $\text{Sr}_2\text{RuO}_4$  and the  $\text{Sr}_3\text{Ru}_2\text{O}_7$  side of the superlattice. B3 and B4 are the inner RuO layers in the  $\text{Sr}_3\text{Ru}_2\text{O}_7$  part. M1 and M2 indicate the interface and the inner RuO layers within the  $\text{Sr}_2\text{RuO}_4$  side. A schematic view of the structure and the labels is reported in Fig. 4b.

orbital	$\text{Sr}_3\text{Ru}_2\text{O}_7$										Interface		$\text{Sr}_2\text{RuO}_4$							
	B4-B3		B3		B3-B2		B2		B2-B1		B1		B1-M1		M1		M1-M2		M2	
	$[lmn]$	$[00p]$	$[000]$	$[100]$	$[\frac{1}{3}\frac{1}{3}\frac{1}{3}]$		$[000]$	$[100]$	$[00p]$	$[000]$	$[100]$	$[\frac{1}{3}\frac{1}{3}\frac{1}{3}]$	$[000]$	$[100]$	$[\frac{1}{3}\frac{1}{3}\frac{1}{3}]$	$[000]$	$[100]$	$[000]$	$[100]$	
xy-xy	-0.015	-0.423	-0.235		0.002/0.001	-0.423	-0.235	-0.016	-0.424	-0.237	0.002	-0.490	-0.380	0.002	-0.491	-0.381				
yz-xy	0	0	$\pm 0.001$		0.006/0.004/0.003	0	$\pm 0.001$	0	0	$\pm 0.001$	0.006/0.005	0	0	0.006	0	0				
xz-xy	0	0	$\pm 0.016$		0.006/0.004/0.003	0	$\pm 0.016$	0	0	$\pm 0.020$	0.006/0.005	0	0	0.006	0	0				
yz-yz	-0.248	-0.335	-0.008		-0.023/-0.015/-0.011	-0.332	-0.008	-0.244	-0.315	-0.008	-0.021/-0.014	-0.307	-0.039	-0.020	-0.289	-0.039				
yz-xz	0	0	$\pm 0.080$		-0.025/-0.013/-0.003	0	$\pm 0.079$	0	0	$\pm 0.077$	-0.020/-0.009	0	0	-0.015	0	0				
xz-xz	-0.248	-0.335	-0.285		-0.023/-0.015/-0.011	-0.332	-0.285	-0.244	-0.315	-0.277	-0.021/-0.014	-0.307	-0.280	-0.020	-0.289	-0.273				

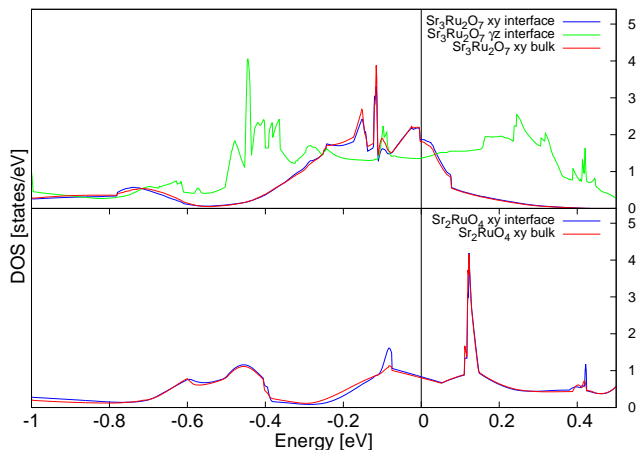


FIG. 6: The projected density of states for the 4d bands of the Ru atoms placed at different layers within the HET42 heterostructure for the  $\text{Sr}_3\text{Ru}_2\text{O}_7$  (top panel) and  $\text{Sr}_2\text{RuO}_4$  (bottom panel) sides. The blue line represents the  $d_{xy}$  DOS for Ru atoms at the interface, the red lines the DOS in the inner layers. The Fermi energy is set to zero.

tronic properties within the superlattice and with respect to the bulk  $\text{Sr}_2\text{RuO}_4$  and  $\text{Sr}_3\text{Ru}_2\text{O}_7$  we have determined, starting from the outcome of the density functional analysis, the effective tight-binding Hamiltonian in the ML-WFs basis. The output of the relevant electronic parameters connecting the Ru  $t_{2g}$ -like Wannier states is given in the Table VI for the case of the HET33 heterostructure. This is the more general case as it contains inequivalent inner RuO layers for both the  $\text{Sr}_2\text{RuO}_4$  and  $\text{Sr}_3\text{Ru}_2\text{O}_7$  subsystems. Starting from the  $\text{Sr}_3\text{Ru}_2\text{O}_7$  side of the heterostructure we notice that the electronic parameters are quite homogeneous within the superlattice confirming the small variations in the DOS at the interface and in the inner RuO layers. In particular, the small modification of the local crystal field splitting, the bilayer splitting, and

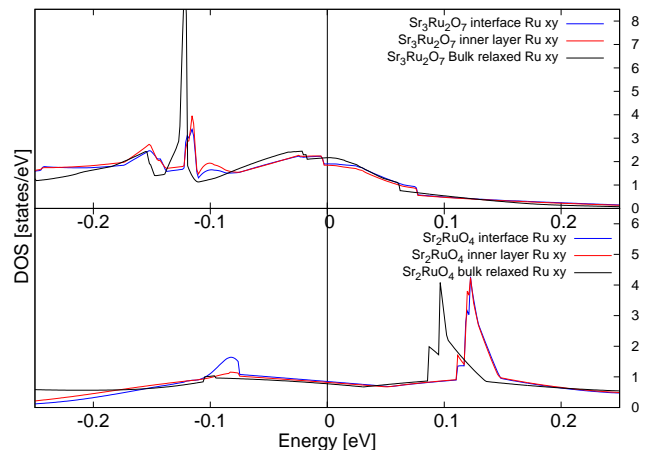


FIG. 7: Bulk vs heterostructure projected density of states for the Ru  $xy$  band. The Fermi energy is set to zero.

the  $t_{2g}$  bandwidth have a trend that follows the main structural changes. Indeed, since the octahedra are flattened for the outer RuO layers at the interface (denoted as B1 and B2 in Fig. 4b) with respect to those in the inner layers (denoted as B3 and B4 in Fig. 4b) the energy associated to the  $d_{\gamma z}$ -like Wannier states is pushed up while the  $d_{xy}$  is not modified. Thus, the overall effect is to reduce the crystal field splitting, i.e.  $\Delta_{cf} = |E_{xy} - E_{\gamma z}|$ , at the interface with respect to the  $\text{Sr}_3\text{Ru}_2\text{O}_7$  inner side of the superlattice. On the other hand, the bilayer splitting, the  $t_{2g}$  in-plane and out-of-plane nearest-neighbour hopping are basically uniform within the superlattice exhibiting a variation in a energy window of 2-10 meV. In such energy range the most significant modification is represented by the increase of the Ru-Ru  $\gamma z$  nearest-neighbour hopping when moving from the interface to the inner layers. It is also worth noticing that the hybridization amplitude between the  $xy$  and  $\gamma z$  Wannier

states is larger in the RuO layers at the interface with the  $\text{Sr}_2\text{RuO}_4$  than in the inner ones. At this point it is also relevant to analyze the differences of the effective tight-binding Hamiltonian between the superlattice  $\text{Sr}_3\text{Ru}_2\text{O}_7$  side and the corresponding bulk phase. By inspection of the Table II we notice that, due to a larger tilting of the octahedra with respect to the bulk, the in-plane  $xy$  Ru-Ru nearest-neighbor hopping is reduced in the superlattice. There occurs also a decrease of the  $\gamma z$  Ru-Ru nearest-neighbor hopping but this is mainly driven by the flattening of the  $\text{RuO}_6$  octahedra in the superlattice. The distortion of the octahedra influences also the crystal field and the bilayer splitting. The energy splitting  $\Delta_{cf}$  is generally reduced in the superlattice if compared to the bulk phase except for the Ru atoms placed in the B1 outer layer of the interface bilayer (see Fig. 4b). The hybridization amplitude between the  $xy$  and  $\gamma z$  Wannier states, which is a relevant parameter in setting the differences between the  $\text{Sr}_2\text{RuO}_4$  and  $\text{Sr}_3\text{Ru}_2\text{O}_7$  electronic structures, is doubled at the interface of the superlattice compared to that for the  $\text{Sr}_3\text{Ru}_2\text{O}_7$  bulk phase.

Let us consider the electronic parameters for the  $\text{Sr}_2\text{RuO}_4$  bulk and in the superlattice. Starting from the crystal field splitting we notice that the elongation of the octahedra at the interface pushes down the energy of the Ru  $\gamma z$  states. Such change, in turn, leads also to an increase of the Ru-Ru in-plane nearest-neighbor hopping moving from the inner layers to the interface ones. The remaining tight-binding parameters keep the symmetry connections as in the  $\text{Sr}_2\text{RuO}_4$  bulk phase. Though the presence of a structural rearrangement at the  $\text{Sr}_2\text{RuO}_4$ - $\text{Sr}_3\text{Ru}_2\text{O}_7$  interface leads to flattening and rotation of the octahedra there are no extra induced hybridizations between the  $t_{2g}$ -like Wannier states. The comparison of the effective tight-binding Hamiltonian between the  $\text{Sr}_2\text{RuO}_4$  side of the superlattice and the corresponding bulk phase shows that the in-plane  $xy$  Ru-Ru nearest-neighbor hopping is slightly reduced in the superlattice and the same happens of the  $\gamma z$  orbitals. Hence, apart from a renormalization of the  $t_{2g}$  bandwidth and a modification of the crystal field splitting the electronic structure in the  $\text{Sr}_2\text{RuO}_4$  keeps its qualitative features as far as it concerns, for instance, the nesting and the presence of the VHSs.

#### IV. CONCLUSIONS

In conclusion by means of first-principles density functional theory we determined the structural and electronic properties of different configurations of superlattices made with  $\text{Sr}_2\text{RuO}_4$  and  $\text{Sr}_3\text{Ru}_2\text{O}_7$  unit cells. Such analysis has been then exploited to construct the effective tight-binding Hamiltonian in the MLWFs basis in order to compare the relevant electronic parameters that determine the dispersions of the  $t_{2g}$ -like states close to the Fermi level.

We have shown that, due to the different symmetry

and size of the  $n=1$  and  $n=2$  unit cells, a rearrangement of the atomic position takes place both within the Ru-O and Sr-O layers. The  $\text{RuO}_6$  octahedra at the  $\text{Sr}_2\text{RuO}_4$ - $\text{Sr}_3\text{Ru}_2\text{O}_7$  interface get elongated in the  $\text{Sr}_2\text{RuO}_4$  side and flattened in the  $\text{Sr}_3\text{Ru}_2\text{O}_7$  along the  $c$ -axis when compared to the octahedra in the inner layers block and those in the bulk phases as well. Another interesting feature is the observation of a misalignment of Sr atoms with respect to the O atoms in the Sr-O blocks at the  $\text{Sr}_2\text{RuO}_4$ - $\text{Sr}_3\text{Ru}_2\text{O}_7$  interface. The effect is not symmetric in amplitude on the two sides of the superlattice at the interface. Furthermore, we have demonstrated that similar structural changes occur also in the RuO layers close to the interface and that they influence the Ru-O-Ru angle resulting into a less pronounced rotation of the  $\text{Sr}_3\text{Ru}_2\text{O}_7$  octahedra.

Concerning the electronic structure, the analysis via the MLWFs approach allowed to extract all the relevant features for the hopping and on-site energies amplitude within the superlattice and in comparison with the corresponding bulk phases. The overall view is that the electronic parameters are quite uniform in the superlattice exhibiting small differences between the interface and inner Ru bands. Furthermore, the symmetry allowed hopping in the superlattice are analogue to those in the  $\text{Sr}_2\text{RuO}_4$  and  $\text{Sr}_3\text{Ru}_2\text{O}_7$  bulk phases. This implies that, for instance, the nesting of the  $\gamma z$  is not affected qualitatively in the  $\text{Sr}_2\text{RuO}_4$  side as well as the presence and the character of the VHSs.

Let us consider the connection between the presented results and the possible experimental consequences. The first observation is that the resulting DOS for the Ru  $xy$  band at the interface in the  $\text{Sr}_2\text{RuO}_4$  side turns out to be greater than that in the bulk  $\text{Sr}_2\text{RuO}_4$ . Still, the reduction of the bandwidth of the Ru  $xy$  band in the superlattice would point towards an enhancement of the correlations at the interface. Those aspects both indicate a tendency to increase the superconducting critical temperature either viewed in a Bardeen-Cooper-Schrieffer scenario or in a correlated driven pairing. Still, the increase of the DOS at the Fermi level and the change in the effective bandwidth can also lead to a ferromagnetic instability within a Stoner picture thus one cannot rule out at this level of description the possibility that the superlattice can exhibit a ferromagnetic transition. So far, the eutectic systems are the only available  $\text{Sr}_2\text{RuO}_4$ - $\text{Sr}_3\text{Ru}_2\text{O}_7$  heterostructure where recent electric transport and muons measurements in the  $\text{Sr}_2\text{RuO}_4$ - $\text{Sr}_3\text{Ru}_2\text{O}_7$  eutectic have confirmed the occurrence of superconductivity at a temperature that is higher than that observed in the *pure*  $\text{Sr}_2\text{RuO}_4$  with an onset of about 2.5 K.<sup>21</sup> Concerning the  $\text{Sr}_3\text{Ru}_2\text{O}_7$  side, we have shown that the VHS is shifted towards the Fermi level in the superlattice if compared to the bulk phase. The closeness of the VHS to the Fermi energy is known to lead to a reduction of the metamagnetic critical field if analyzed in the framework of a weakly correlated approach to the metamagnetic instability<sup>50</sup>. Such observation can be used to under-

stand the origin of the metamagnetism in the  $\text{Sr}_3\text{Ru}_2\text{O}_7$  with respect to the presence of the VHS as well as the limits of a Stoner scenario to address the response upon an applied magnetic field.

### Acknowledgments

We acknowledge useful discussions with G. Cantele and E. Pavarini. Carmine Autieri acknowledges financial

support from "Fondazione Angelo Della Riccia". The research leading to these results has received funding from the EU -FP7/2007-2013 under grant agreement N. 264098 - MAMA.

- 
- <sup>1</sup> H. Y. Hwang, Y. Iwasa, M. Kawasaki, B. Keimer, N. Nagao, and Y. Tokura, *Nature Mat.* **11**, 103 (2012).
- <sup>2</sup> M. Imada, A. Fujimori, and Y. Tokura, *Rev. Mod. Phys.* **70**, 1039 (1998).
- <sup>3</sup> J. Heber, *Nature* **459**, 2830 (2009).
- <sup>4</sup> A. Ohtomo, D. A. Muller, J. L. Grazul, and H. Y. Hwang, *Nature* **419**, 378380 (2002).
- <sup>5</sup> A. Gozar, *Nature* **455**, 782785 (2008).
- <sup>6</sup> A. Ohtomo and H. Y. Hwang, *Nature* **427**, 423426 (2004).
- <sup>7</sup> N. Nakagawa, H. Y. Hwang, and D. A. Muller, *Nature Mater.* **5**, 204209 (2006).
- <sup>8</sup> Y. Tokura and H. Y. Hwang, *Nature Mater.* **7**, 694695 (2008).
- <sup>9</sup> E. Dagotto, *Science* **318**, 1076 (2007).
- <sup>10</sup> Y. Maeno, H. Hashimoto, K. Yoshida, S. Nishizaki, T. Fujita, J. G. Bednorz, and F. Lichtenberg, *Nature* **372**, 532 (1994).
- <sup>11</sup> S. Ikeda, Y. Maeno, S. Nakatsuji, M. Kosaka, and Y. Uwatoko, *Phys. Rev. B* **62**, R6089 (2000).
- <sup>12</sup> R. S. Perry, L. M. Galvin, S. A. Grigera, L. Capogna, A. J. Schofield, A. P. Mackenzie, M. Chiao, S. R. Julian, S. I. Ikeda, S. Nakatsuji, Y. Maeno, *Phys. Rev. Lett.* **86**, 2661 (2001).
- <sup>13</sup> S. A. Grigera, R. S. Perry, A. J. Schofield, M. Chiao, S. R. Julian, G. G. Lonzarich, S. I. Ikeda, Y. Maeno, A. J. Millis, and A. P. Mackenzie, *Science* **294**, 329 (2001).
- <sup>14</sup> G. Cao, L. Balicas, W. H. Song, Y. P. Sun, Y. Xin, V. A. Bondarenko, J. W. Brill, S. Parkin, and X. N. Lin, *Phys. Rev. B* **68**, 174409 (2003).
- <sup>15</sup> Z. Q. Mao, M. Zhou, J. Hooper, V. Golub, and C. J. O'Connor, *Phys. Rev. Lett.* **96**, 077205 (2006).
- <sup>16</sup> R. Gupta, M. Kim, H. Barath, S. L. Cooper, and G. Cao, *Phys. Rev. Lett.* **96**, 067004 (2006).
- <sup>17</sup> P. B. Allen, H. Berger, O. Chauvet, L. Forro, T. Jarlborg, A. Junod, B. Revaz, and G. Santi, *Phys. Rev. B* **53**, 4393 (1996).
- <sup>18</sup> R. Fittipaldi, A. Vecchione, S. Fusanobori, K. Takizawa, H. Yaguchi, J. Hooper, R. S. Perry, and Y. Maeno, *J. Cryst. Growth* **282**, 152 (2005).
- <sup>19</sup> R. Ciancio, H. Petterson, J. Brjesson, S. Lopatin, R. Fittipaldi, A. Vecchione, S. Kittaka, Y. Maeno, S. Pace, and E. Olsson, *Appl. Phys. Lett.* **95**, 142507 (2009).
- <sup>20</sup> R. Fittipaldi, D. Sisti, A. Vecchione, S. Pace, *Cryst. Growth and Design*, **7**, 2495 (2007).
- <sup>21</sup> T. Shiroka *et al.*, *Phys. Rev. B* **85**, 134527 (2012).
- <sup>22</sup> J. Hooper, M. Zhou, Z. Q. Mao, Y. Liu, R. S. Perry, and Y. Maeno, *Phys. Rev. B* **73**, 132510 (2006).
- <sup>23</sup> R. Fittipaldi, A. Vecchione, R. Ciancio, S. Pace, M. Cuoco, D. Stornaiuolo, D. Born, F. Tafuri, E. Olsson, S. Kittaka, H. Yaguchi, and Y. Maeno, *Europhys. Lett.* **83**, 27007 (2008).
- <sup>24</sup> M. A. Zurbuchen, Y. Jia, S. Knapp, A. H. Carim, D. G. Schlom, L. Zou, and Y. Liu, *Appl. Phys. Lett.* **78**, 2351 (2001); M. A. Zurbuchen, Y. Jia, S. Knapp, A. H. Carim, D. G. Schlom, and X. Q. Pan, *Appl. Phys. Lett.* **83**, 3891 (2003).
- <sup>25</sup> W. Tian, J. H. Haeni, D. G. Schlom, E. Hutchinson, B. L. Sheu, M. M. Rosario, P. Schiffer, Y. Liu, M. A. Zurbuchen, and X. Q. Pan, *Appl. Phys. Lett.* **90**, 022507 (2007).
- <sup>26</sup> Y. Krockenberger *et al.*, *Appl. Phys. Lett.* **97**, 082502 (2010).
- <sup>27</sup> P. Hohenberg and W. Kohn, *Phys. Rev.* **136**, B864 (1964), W. Kohn and L. J. Sham, *Phys. Rev.* **140**, 1133 (1964).
- <sup>28</sup> X. Gonze, G. M. Rignanese, M. Verstraete, J. M. Beuken, Y. Pouillon, R. Caracas, F. Jollet, M. Torrent, G. Zerah, M. Mikami, P. Ghosez, M. Veithen, J. Y. Raty, V. Olevano, F. Bruneval, L. Reining, R. Godby, G. Onida, D. R. Hamann, and D. C. Allan, *Zeit. Kristallogr.* **220**, 558 (2005).
- <sup>29</sup> Z. Wu and R. E. Cohen, *Phys. Rev. B* **73**, 235116 (2006).
- <sup>30</sup> M. Fuchs, M. Scheffler, *Comput. Phys. Commun.* **119**, 67 (1999).
- <sup>31</sup> D. I. Bilc and Ph. Ghosez *et al.*, *Phys. Rev. B* **77**, 165107 (2008).
- <sup>32</sup> J. P. Perdew, K. Burke, and M. Ernzerhof, *Phys. Rev. Lett.* **77**, 3865 (1996).
- <sup>33</sup> A. A. Mostofi, J. R. Yates, Y. S. Lee, I. Souza, D. Vanderbilt, and N. Marzari, *Comput. Phys. Commun.*, **178**, 685 (2008).
- <sup>34</sup> N. Marzari and D. Vanderbilt, *Phys. Rev. B* **56**, 12847 (1997).
- <sup>35</sup> I. Souza, N. Marzari, and D. Vanderbilt, *Phys. Rev.* **65**, 035109 (2001).
- <sup>36</sup> T. Oguchi, *Phys. Rev. B* **51**, 1385 (1995).
- <sup>37</sup> D. J. Singh, *Phys. Rev. B* **52**, 1358 (1995).
- <sup>38</sup> I. I. Mazin and D. J. Singh, *Phys. Rev. Lett.* **82**, 4324 (1999).
- <sup>39</sup> A. Liebsch and A. Lichtenstein, *Phys. Rev. Lett.* **84**, 1599 (2000).
- <sup>40</sup> E. Pavarini and I. Mazin, *Phys. Rev. B* **74**, 035115 (2006).
- <sup>41</sup> R. Matzdorf, Z. Fang, Ismail, Jiandi Zhang, T. Kimura, Y. Tokura, K. Terakura, and E. W. Plummer, *Science* **289**, 746 (2000).
- <sup>42</sup> A. Tamai, M. P. Allan, J. F. Mercure, W. Meevasana, R. Dunkel, D. H. Lu, R. S. Perry, A. P. Mackenzie, D. J. Singh, Z. X. Shen, and F. Baumberger,

- Phys. Rev. Lett. **101**, 026407 (2008).
- <sup>43</sup> A.V. Puchkov, Z.-X. Shen, and G. Cao, Phys. Rev. B **58**, 6671 (1998).
- <sup>44</sup> D. J. Singh and I. I. Mazin Phys. Rev. B **63**,165101 (2001).
- <sup>45</sup> Q. Huang J. W. Lynn and R. W. Erwin J. Jarupatrakorn and R. J. Cava Phys. Rev. B **58**, 8515 (1998).
- <sup>46</sup> J. C. Slater and G. F. Koster, Phys. Rev. **94**, 1498-1524 (1954).
- <sup>47</sup> C. Piefke and F. Lechermann Phys. Status Solidi B **248**, 2269 (2011).
- <sup>48</sup> O. Chmaisnen, J. D. Jorgensen, H. Shaked, S. Ikeda, and Y. Maeno, Phys. Rev. B **57**, 5067 (1998).
- <sup>49</sup> X. Gonze, B. Amadon, P. M. Anglade, J. M. Beuken, F. Bottin, P. Boulanger, F. Bruneval, D. Caliste, R. Caracas, M. Cote, T. Deutsch, L. Genovese, P. Ghosez, M. Giantomassi, S. Goedecker, D. R. Hamann, P. Hermet, F. Jollet, G. Jomard, S. Leroux, M. Mancini, S. Mazevet, M. J. T. Oliveira, G. Onida, Y. Pouillon, T. Rangel, G. M. Rignanese, D. Sangalli, R. Shaltaf, M. Torrent, M. J. Verstraete, G. Zerah, J. W. Zwanziger, Computer Phys. Comm. **180**, 2582 (2009).
- <sup>50</sup> C. Autieri, M. Cuoco, and C. Noce, Phys. Rev. B **85**, 075126 (2012).